frontiers | Frontiers in Earth Science

ORIGINAL RESEARCH
published: 10 May 2022
doi: 10.3389/feart.2022.824348

Impact of Fractal Features on Gas Adsorption and Desorption Capacities and Ad-/Desorption Hysteresis in Coals Based on Synchrotron Radiation SAXS

Yixin Zhao[1,2], Chujian Han[1], Yingfeng Sun[3,4,5], Yirui Gao[1], Haiqing Qiao[1] and Zhenyu Tai[1]*

[1]School of Energy and Mining Engineering, China University of Mining and Technology, Beijing, China, [2]Beijing Key Laboratory for Precise Mining of Intergrown Energy and Resources, China University of Mining and Technology, Beijing, China, [3]Research Institute of Macro-Safety Science, University of Science and Technology Beijing, Beijing, China, [4]School of Civiland Resource Engineering, University of Science and Technology Beijing, Beijing, China, [5]Key Laboratory of Deep Earth Science and Engineering (Sichuan University), Ministry of Education, Chengdu, China

OPEN ACCESS

Edited by:
Yiwen Ju,
University of Chinese Academy of Sciences, China

Reviewed by:
Jianhong Kang,
China University of Mining and Technology, China
Mengdi Sun,
Northeast Petroleum University, China

***Correspondence:**
Yixin Zhao
zhaoyx@cumtb.edu.cn

Specialty section:
This article was submitted to Economic Geology, a section of the journal Frontiers in Earth Science

Received: *29 November 2021*
Accepted: *21 March 2022*
Published: *10 May 2022*

Citation:
Zhao Y, Han C, Sun Y, Gao Y, Qiao H and Tai Z (2022) Impact of Fractal Features on Gas Adsorption and Desorption Capacities and Ad-/Desorption Hysteresis in Coals Based on Synchrotron Radiation SAXS. Front. Earth Sci. 10:824348. doi: 10.3389/feart.2022.824348

Gas adsorption and desorption capacities and ad-/desorption hysteresis in coal are important for carbon capture and storage (CCS) and coalbed methane (CBM) development. To investigate the impact of fractal features on gas adsorption and desorption capacities and ad-/desorption hysteresis in coals, five coal samples were collected and carried out methane (CH_4) and CO_2 isothermal ad-/desorption experiments. Small angle X-ray scattering (SAXS) was applied to characterize the fractal features of the coal pore structure. The results show that five coal samples show surface fractal features, represented by surface fractal dimension (D_s). The adsorption and desorption capacities of CO_2 are stronger than those of CH_4. In the adsorption stage, D_s and Langmuir adsorption volume ($V_{L\text{-}ad}$) show a positive relationship for CH_4 and CO_2, due to the van der Waals force and available adsorption sites. In the desorption stage, D_s and Langmuir desorption volume ($V_{L\text{-}de}$) show a positive relationship for CH_4 and CO_2, because most adsorbed gas molecules can desorb and diffuse out of the pores when gas pressure decreases. No obvious correlation was found between D_s and Langmuir adsorption pressure ($P_{L\text{-}ad}$) as well as between D_s and Langmuir desorption pressure ($P_{L\text{-}de}$) for CO_2 and CH_4. An improved hysteresis index (IHI) was adopted to characterize the degree of gas ad-/desorption hysteresis. The IHI values of CO_2 vary from 12.2 to 35.2%, and those of CH_4 vary from 8.9 to 50.3%. The curves of D_s vs. IHI for CO_2 and CH_4 are like an irreversible "V" shape, which yields to be further studied. This work further extends SAXS application in exploring the impact of coal pore structure on gas adsorption related phenomena, which is beneficial for CCS technology and CBM development.

Keywords: SAXS, fractal, adsorption, desorption, hysteresis, coal

INTRODUCTION

In the context of carbon emission peaks and carbon neutral in China, carbon capture and storage (CCS) has become a research hotspot (Budinis et al., 2018; Fan et al., 2018). International Energy Agency (IEA) pointed out that if the warming rate by the end of this century is about to achieve 1.75°C, the CCS technology needs to contribute 32% of CO_2 emission reduction (IEA, 2017). Coalbed methane (CBM) is a typically geological gas mainly consisting of methane (CH_4), which contains huge energy and thus serves as an emerging energy resource (Wang et al., 2014; Zhang et al., 2016). In 2020, CBM production is 58.2×10^8 cubic meters, which is of great significance to ensure energy security and reduce foreign dependence on natural gas (Xu et al., 2021). Gas in coal has three occurrence states: dissolution state, adsorption state, and free state, respectively, and the majority of gases are in the adsorption state (Cui et al., 2004). Ad-/desorption isotherms can quantitatively reflect the gas adsorption and desorption capacities in coal; meanwhile, it has been observed that it exists a positive difference between the ad-/desorption isotherms for CH_4 and CO_2, which is termed as adsorption–desorption hysteresis (Wang G. et al., 2016), sorption hysteresis (Ekundayo and Rezaee, 2019; He et al., 2020), desorption hysteresis (Ma et al., 2012), and degree of irreversibility (Zhang and Liu, 2017) and so on in different literature. In this work, the authors adopted the term—ad-/desorption hysteresis—to describe this difference for the sake of unification. For CCS technology, coal reservoirs have been proven to be a viable CSS geological body, with a CO_2 storage ability of 12 Gt (Liu et al., 2005). As is well known, CO_2 adsorption and desorption features are closely related to the amount and stability of CO_2 storage (Sun et al., 2018). Similarly, in CBM industry, CH_4 adsorption and desorption properties directly affect CBM production, the larger the amount of CH_4 that can be desorbed is, the higher the recovery rate is, whereas the ad-/desorption hysteresis can hinder the recovery rate (Ma et al., 2012).

The pore structure is one of the key factors affecting gas adsorption, desorption, and ad-/desorption hysteresis in coal (Tan et al., 2018; Yin et al., 2019; Zhou et al., 2020) because the pore structure is where the gas is adsorbed and desorbed. Fractal dimension is a parameter that can comprehensively reflect the features of coal pore structure (Liu and Nie, 2016). In recent years, some scholars just tentatively began to adopt fractal theory to explore the intrinsic mechanism of gas adsorption-related phenomena. Li et al. (2015) stated that based on the fractal dimension tested by N_2 adsorption, the CH_4 adsorption capacity enhances with surface fractal dimension increasing but weakens with pore fractal dimension increasing. However, similarly based on the N_2 adsorption method, Sun et al. (2015) drew a conclusion that is not fully consistent with Li et al. (2015), reporting that the CH_4 adsorption capacity increases with the increase of surface fractal dimension, but there is no obvious relationship between CH_4 adsorption capacity and pore fractal dimension. Niu et al. (2019) applied three different measurement methods, including N_2 adsorption, SAXS, and scanning electron microscopy to research the effect of fractal dimension on CH_4 adsorption behavior, and found that Langmuir adsorption pressure shows a negative relationship with fractal dimension. He et al. (2020) applied CO_2 and N_2 adsorption methods to calculate the fractal dimension and analyzed the relevancy between the fractal dimension and methane sorption hysteresis in coal, and found that there is a potential positive correlation between the methane sorption hysteresis and the coal heterogeneity. In summary, even though if any, research on the combination of fractal and gas adsorption related phenomena remains to be scarce and unsystematic; meanwhile, the characterization of fractal dimension in previous studies mainly relies on traditional gas adsorption methods.

As a non-destructive testing technology, synchrotron radiation Small Angle X-Ray Scattering (SAXS) has been extensively applied to measure the pore structure of multiporous materials (Mares et al., 2009; Syed et al., 2018); it can concurrently measure both open and closed pores in its testing scope (Pan et al., 2016; Zhao et al., 2019). As a relatively novel and innovative method for pore structure measurement, SAXS application has gradually extended to the field of coal fractal feature characterization. Zhao and Peng, (2017) used SAXS to test the fractal of six coal samples with different ranks, and found that coal samples show surface fractal at the region of low q value and pore fractal at the region of high q value. Song et al. (2014) found that the surface fractal dimension of coal tested by SAXS increases with the increase in deformation extent. Nie et al. (2021) found that when gas adsorption occurs in coal, the transformation of the coal pore structure can be characterized by fractal dimension tested by SAXS. Xie et al. (2019) conducted SAXS fractal experiments on bituminous coal and stated that the bituminous coal shows surface fractal features throughout the carbonization process. Wang et al. (2021) conducted SAXS fractal experiments on anthracite coal and demonstrated that with the development of carbonization, the fractal feature of the coal pore structure varies between pore fractal and surface fractal. However, research on the correlation between the fractal dimension on the basis of SAXS fractal theory and gas adsorption related phenomena in coal is relatively scarce. Accordingly, it is greatly necessary to enhance and expand the application of SAXS fractal theory to the investigation of gas adsorption and desorption and ad-/desorption hysteresis in coal.

In this work, five coal samples were performed on SAXS experiments and adsorption and desorption isothermal experiments. Their surface fractal dimensions were calculated based on the SAXS fractal theory, their adsorption and desorption capacities were quantified by Langmuir constants, the degrees of their ad-/desorption hysteresis were quantified by a hysteresis index, and the impact of coal fractal features on gas adsorption and desorption capacities and ad-/desorption hysteresis was investigated.

EXPERIMENTAL SETUP

Sampling and Sample Preparation

In this work, five experimental samples were collected from five different mines. Sampling sites and properties of coal samples were listed in **Table 1**. The mean maximum vitrinite reflectance ($R_{o,max}$) is from 0.68 to 4.33%, covering low-rank, middle-rank,

TABLE 1 | Sampling sites and properties of samples.

Sample Number	Sampling from	$R_{o,max}$ (%)	Proximate analysis (%)				Maceral content (%)			
			M	*V*	*Fc*	*A*	*Vit.*	*Ine.*	*Exi.*	*Min.*
#1	No. 4 seam in Yanya mine	0.68	1.20	26.41	51.87	20.84	36.4	22.1	32.5	9.0
#2	No. 9 seam in Tangshan mine	1.12	1.60	32.83	56.88	8.71	61.6	19.3	1.6	17.5
#3	No. 2 seam in Hongling mine	1.77	0.58	18.57	73.24	9.48	73.5	24.1	0	2.4
#4	No. 3 seam in Yuwu mine	2.07	1.02	10.76	75.20	13.27	81.6	11.4	0	7.0
#5	No. 3 seam in Changzhen mine	4.33	1.18	9.51	76.79	14.15	91.0	7.5	0	1.5

Vit., vitrinite; Ine., inertinite; Exi., exinite; Min., mineral; M, moisture; V, volatile; Fc, fixed carbon; A, ash.

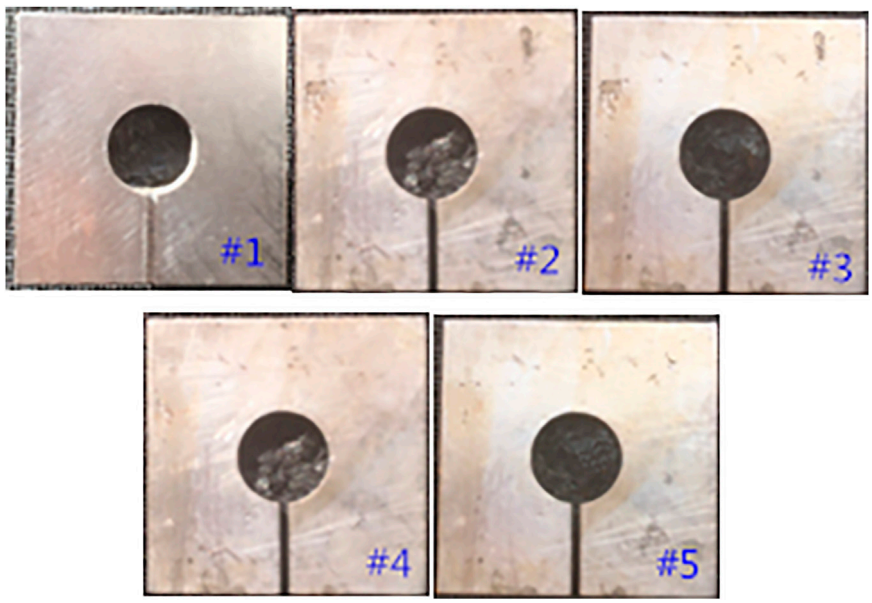

FIGURE 1 | Coal slices processed for SAXS experiments.

and high-rank coals. The moisture content (*M*) ranges from 0.58 to 1.60%, the volatile content (*V*) ranges from 9.51 to 32.83%, the fixed carbon content (*Fc*) ranges from 51.87 to 76.79%, and the ash content (*A*) ranges from 8.71 to 20.84%. The mineral content of sample #2 (17.5%) is the highest and that of sample #5 (1.5%) is the lowest, the vitrinite group content of sample #5 (91.0%) is the highest and that of sample #1 (36.4%) is the lowest, and the exinite contents of samples #3, #4 and #5 are 0.

For SAXS experiments, the first step is to process samples into round slices with a thickness of 0.5 mm and a diameter of 9.5 mm, as shown in **Figure 1**, and then a sample chamber, which was specifically covered by Kapton film, was used to contain the processed samples for the following experiment.

For gas isothermal ad-/desorption measurements, samples were pulverized into 60–80 meshes (180–250 μm), and about 10 g of pulverized samples was selected to be degassed at 30°C for 24 h and heated 1 h to fully remove the moisture inside samples.

Synchrotron SAXS Experiments

Beijing Synchrotron Radiation Facilities (BSRF) were applied to conduct SAXS experiments in this work. The authors have described the parameters of BSRF in detail in our previous research (Zhao et al., 2014).

For SAXS experiments, the chamber loaded with samples was placed on the sample table, 1,650 mm far away from the detector, and then the SAXS device was started to record the photodiode readings and collect SAXS images; this process lasted for about 5 s. And then the FIT2D software was applied to convert the SAXS images into one-dimensional scattering data (Hammersley et al., 1996). The authors have given the details of SAXS image processing in the FIT2D software in our previous research (Zhao et al., 2019).

Gas Isothermal Ad-/Desorption Experiments

An H-Sorb sorption device (Sun et al., 2020) was used for CO_2 and CH_4 adsorption and desorption experiments. The processed samples were first loaded into an adsorption tank and evacuated, and the remaining volume of the adsorption tank was measured. Then, a certain volume of gas was charged into the adsorption tank or discharged from the adsorption tank until the pressure in

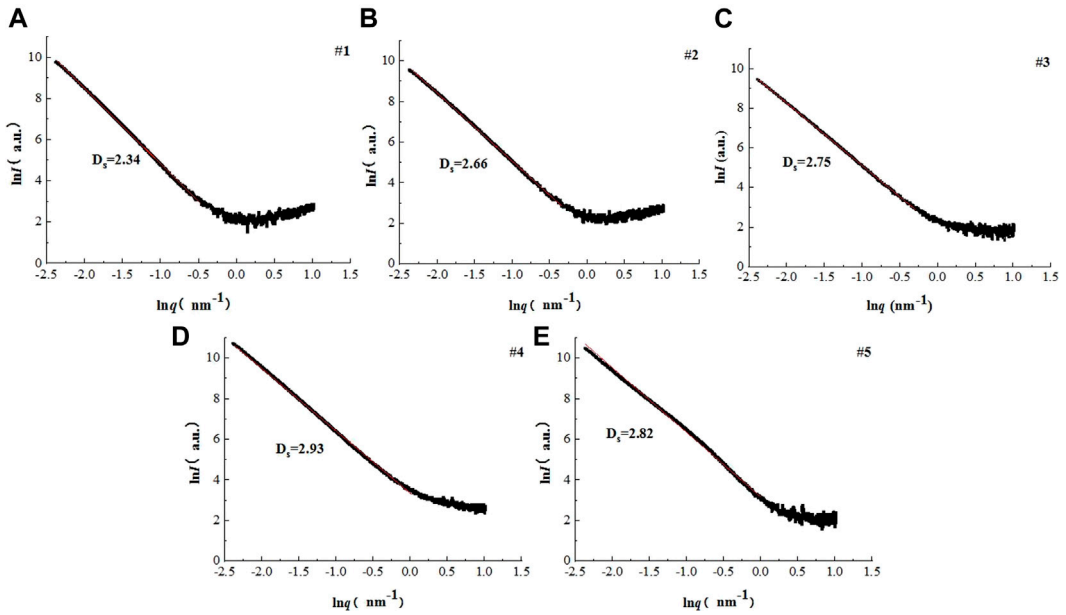

FIGURE 2 | Fractal curves. **(A)** Sample #1, **(B)** Sample #2, **(C)** Sample #3, **(D)** Sample #4, and **(E)** Sample #5.

each section reached an equilibrium state. At this moment, part of gas was adsorbed, and part of gas was still in the remaining volume in the free state. The volume of gas charged was known, and the free volume after deducting the remaining volume was the adsorption volume in samples. Repeat the above procedures to obtain the adsorption volume in each pressure section. The adsorption isotherms were obtained when the gas was charged into the adsorption tank from low pressure to high pressure, and the desorption isotherms were obtained when the gas was discharged out of the adsorption tank from high pressure to low pressure.

RESULTS AND DISCUSSION

Fractal Characterization by SAXS

Wijnen et al. (1991) have ever found that the power-law formula can well express the SAXS intensity of a fractal object,

$$I(q) = I_0 q^{-\alpha}, \tag{1}$$

where α varies from 0 to 4, serving as the fractal parameter.

The fractal features of the coal pore structure are defined as surface fractal and pore fractal based on the SAXS fractal theory, which are represented by D_s and D_p, respectively. If α is between 3 and 4, the pore structure is of surface fractal feature, and the value of D_s is D_s = 6-α. If α is between 0 and 3, the pore structure is of pore fractal feature, and the value of D_p is $D_p = \alpha$ (Reich et al., 1992).

Figure 2 shows the fractal curves of five coal samples. The fractal dimensions were obtained by making a tangent to the ln$I(q)$—ln$q$ curves within linear ranges. The results show that the α values range between 3 and 4, indicating that all samples show surface fractal features. The D_s values vary from 2.34 to 2.93 with sample #4 being of the highest D_s value and sample #1 being of the lowest D_s value, as listed in **Table 2**.

Determination of Langmuir Constants

In this work, the adsorption isotherms are determined by the classic Langmuir formula (Langmuir, 1918) and the desorption isotherms are determined by the modified Langmuir formula (Ma et al., 2011) since it exists residual adsorption volume under a lack pressure between adsorption and desorption isotherms, which is to say that the gas volume is not zero when the pressure decreases to zero in the desorption stage. **Eqs 2**, **3** represent these two models, respectively,

$$V = \frac{PV_{L-ad}}{P + P_{L-ad}}, \tag{2}$$

$$V = \frac{PV_{L-de}}{P + P_{L-de}} + M, \tag{3}$$

where P stands for the equilibrium gas pressure in the adsorption or desorption stage, MPa; V is the adsorbed gas volume when the gas pressure reaches P, ml/g; $V_{L\text{-}ad}$ and $V_{L\text{-}de}$ are the Langmuir adsorption and desorption volumes, which is equal to the maximum monolayer adsorption and desorption values of gas, ml/g; $P_{L\text{-}ad}$ and $P_{L\text{-}de}$ are the Langmuir adsorption and desorption pressures, the pressure when the adsorbed gas volume is half of $V_{L\text{-}ad}$ and $V_{L\text{-}de}$, MPa; and M is the residual adsorption volume under a lack pressure, ml/g.

Figure 3 shows the adsorption and desorption isotherms of CO_2 and CH_4. **Tables 3**, **4** show the Langmuir constants of CO_2 and CH_4, respectively.

As is widely known, the Langmuir volume and Langmuir pressure have a significant impact on gas adsorption and

TABLE 2 | Results of the pore structure properties of coal samples based on SAXS.

Sample	#1	#2	#3	#4	#5
Fractal feature	Surface fractal	Surface fractal	Surface fractal	Surface fractal	Surface fractal
α	3.66	3.34	3.25	3.07	3.18
D_S	2.34	2.66	2.75	2.93	2.82

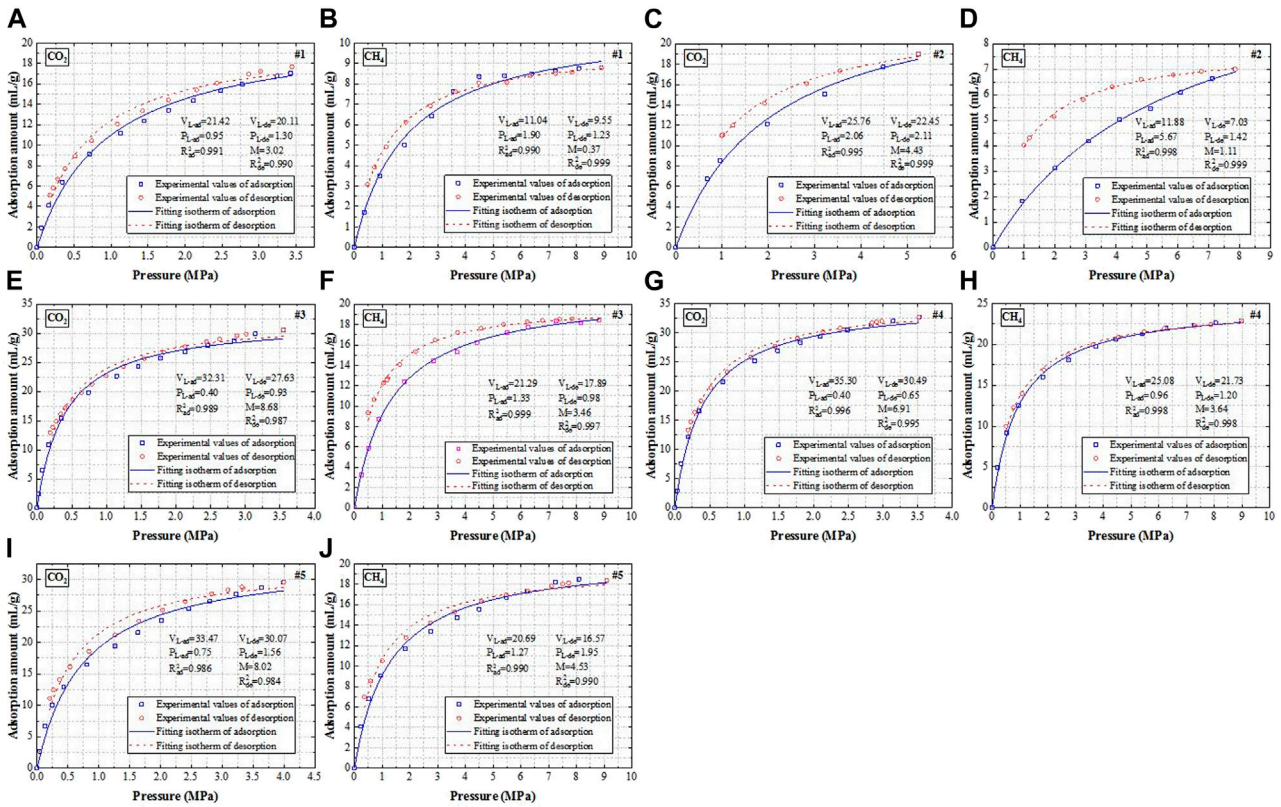

FIGURE 3 | Adsorption and desorption isotherms of CO2 and CH4. **(A-B)** Sample #1, **(C-D)** Sample #2, **(E-F)** Sample #3, **(G-H)** Sample #4, and **(I-J)** Sample #5.

TABLE 3 | Langmuir constants of CO_2.

Sample	CO_2 adsorption		CO_2 desorption		
	$V_{L\text{-}ad}$ (ml/g)	$P_{L\text{-}ad}$ (MPa)	$V_{L\text{-}de}$ (ml/g)	$P_{L\text{-}de}$ (MPa)	M
#1	21.42	0.95	20.11	1.30	3.02
#2	25.76	2.06	22.45	2.11	4.43
#3	32.31	0.40	27.63	0.93	8.68
#4	35.30	0.40	30.49	0.65	6.91
#5	33.47	0.75	30.07	1.56	8.02

TABLE 4 | Langmuir constants of CH_4.

Sample	CH_4 adsorption		CH_4 desorption		
	$V_{L\text{-}ad}$ (ml/g)	$P_{L\text{-}ad}$ (MPa)	$V_{L\text{-}de}$ (ml/g)	$P_{L\text{-}de}$ (MPa)	M
#1	11.04	1.90	9.55	1.23	0.37
#2	11.88	5.67	7.03	1.42	1.11
#3	21.29	1.33	17.89	0.98	3.46
#4	25.08	0.96	21.73	1.20	3.64
#5	20.69	1.27	16.57	1.95	4.53

desorption performance. The higher $V_{L\text{-}ad}$ is, the stronger the gas adsorption capacity is, the higher $P_{L\text{-}ad}$ is, the harder the gas is adsorbed to the coal pore surface; similarly, the higher $V_{L\text{-}de}$ is, the stronger the gas desorption capacity is, the higher $P_{L\text{-}de}$ is, the harder the gas is desorbed to the coal pore surface (Niu et al., 2019). It can be seen from **Tables 3**, **4** that for the same sample, the $V_{L\text{-}ad}$ and $V_{L\text{-}de}$ values of CO_2 are greater than those of CH_4, demonstrating that the adsorption and desorption capacities of CO_2 are stronger than those of CH_4, which is in line with previous studies (Sander et al., 2016; Zhang et al., 2018). This is attributed to the fact that CO_2 owns a smaller kinetic diameter than CH_4 does (CO_2: 0.33 nm versus CH_4: 0.38 nm); therefore, CO_2 is much

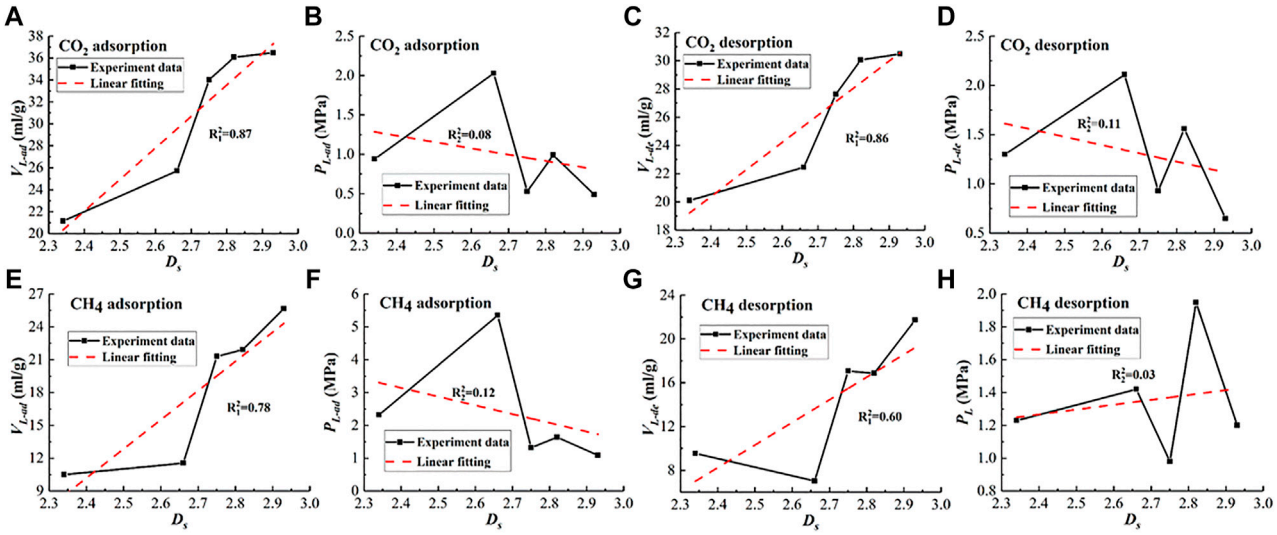

FIGURE 4 | Relationship between D_s and Langmuir constants. **(A)** D_s vs. $V_{L\text{-}ad}$ for CO_2, **(B)** D_s vs. $P_{L\text{-}ad}$ for CO_2, **(C)** D_s vs. $V_{L\text{-}de}$ for CO_2, **(D)** D_s vs. $P_{L\text{-}de}$ for CO_2, **(E)** D_s vs. $V_{L\text{-}ad}$ for CH_4, **(F)** D_s vs. $P_{L\text{-}ad}$ for CH_4, **(G)** D_s vs. $V_{L\text{-}de}$ for CH_4, and **(H)** D_s vs. $P_{L\text{-}de}$ for CH_4.

easier to diffuse into pores with smaller size (Hou et al., 2020), and the affinity of coal matrix to CO_2 is stronger than that of coal matrix to CH_4. Similarly, for the same sample, the $P_{L\text{-}ad}$ value of CH_4 is greater than that of CO_2, indicating that CH_4 is harder to be adsorbed on the coal pore surface than CO_2; nevertheless, there is no obvious rule concerning the $P_{L\text{-}de}$ values.

Impact of D_s on Adsorption and Desorption Capacities

Figure 4 shows D_s vs. Langmuir constants curves. It can be seen from **Figure 4A**, in the CO_2 adsorption stage, $V_{L\text{-}ad}$ increases with D_s increasing, demonstrating that the larger D_s is, the stronger the CO_2 adsorption capacity is. **Figure 4E** shows that in the CH_4 adsorption stage, D_s and $V_{L\text{-}ad}$ show a positive relationship. $V_{L\text{-}ad}$ increases with D_s increasing, demonstrating that the larger D_s is, the stronger the CH_4 adsorption capacity is, which is consistent with studies by Niu et al. (2019) using SAXS and Li et al. (2015) using N_2 adsorption.

The gas adsorption in coal includes monolayer adsorption and multilayer adsorption (Yang and Liu, 2019). In the monolayer adsorption stage, there are two main factors affecting the gas adsorption volume, one is the van der Waals force existing between the pore surface and the gas molecules and the other is the number of adsorption sites available on the pore surface. D_s can represent the strength of the van der Waals force (Chen et al., 2017). The van der Waals force is an indicator of the mutual attraction strength between molecules.

In the adsorption process, gas molecules can diffuse into the pores with a size larger than or equal to the average free path of gas molecules under the effect of gas pressure. The coal matrix can be regarded as organic solids composed of carbon atoms, the gas molecules entered the pore structure can be attracted by the carbon atoms on the pore surface, this is where the van der Waals force works, thereby the gas molecules can earn a tendency to move toward the pore surface. This tendency grants the carbon atoms on the pore surface extra energy—the surface free energy (He et al., 1996). The carbon atoms on the pore surface are always trying to absorb other substances around them to reduce their surface free energy. Hence, the stronger the van der Waals force is, the stronger the gas adsorption performance is. Meanwhile, D_s can also represent the roughness and irregularity of the pore surface (Yao et al., 2008; Niu et al., 2019). The higher D_s value indicates the rougher pore surface, at which more sites are available for gas adsorption (Wang Y. et al., 2016), further enhancing the gas adsorption capacities. Hence, the fact that D_s and $V_{L\text{-}ad}$ show a positive relationship can be explained from the perspectives of the pore surface roughness and the van der Waals force.

However, with the increase of relative pressure, the monolayer adsorption transits to the multilayer adsorption. During the multilayer adsorption stage, more adsorption layers are established, and the adsorbent interface becomes smooth. At this time, the effect of the capillary condensation, which can be represented by D_p, accounts for a leading position (Qi et al., 2002). Unfortunately, SAXS failed to test the pore fractal in this study, leading to counting for the gas amount of multilayer adsorption mainly affected by the pore fractal when we discuss the impact of D_s on the gas adsorption capacities. However, according to Wang (2015), the Langmuir model is based on the hypothesis of monolayer adsorption and its good application in actual projects illustrates that the monolayer adsorption takes up a leading proportion. Besides, since the gas pressure during the adsorption and desorption at normal temperature is much higher than the gas pressure range applicable to the multilayer adsorption, the multilayer adsorption is generally considered to be rather weak. Therefore, although the gas amount of multilayer adsorption is counted into the total gas adsorption

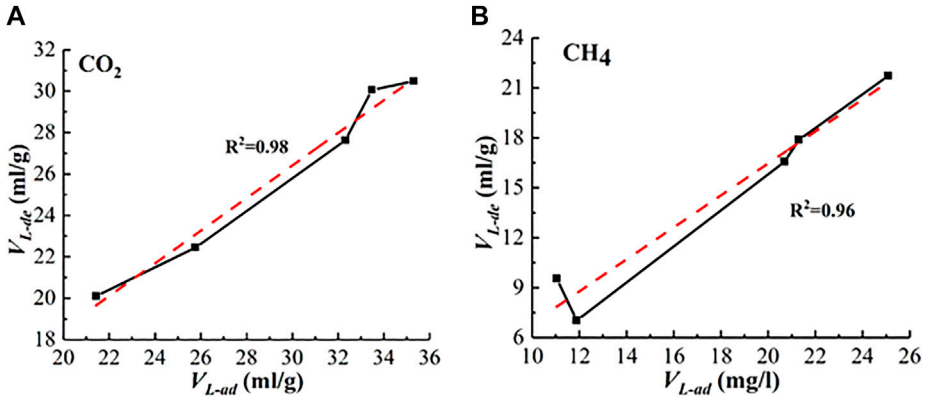

FIGURE 5 | Relationship between $V_{L\text{-}ad}$ and $V_{L\text{-}de}$. **(A)** CO_2, and **(B)** CH_4.

amount, it doesn't actually affect the discussion of the impact of D_s on the gas adsorption capacities.

As shown in **Figures 4C, G**, $V_{L\text{-}de}$ for CO_2 and $V_{L\text{-}de}$ for CH_4 exhibit an increasing trend with the increase of D_s. It can be explained by the fact that $V_{L\text{-}ad}$ shows a positive relationship with $V_{L\text{-}de}$, as demonstrated by **Figure 5**. And as discussed above, larger D_s values represent the rougher pore surface providing more available adsorption sites and stronger van der Waal force reinforcing the mutual attraction strength between the gas molecules and pore surface, which enhances the total adsorption volume in the adsorption stage. On the contrary, in the desorption stage, the van der Waals force plays a role in restricting gas molecules to escape from the pore surface; besides, rougher pore surface produces stronger friction resistance hindering the desorbed gas molecules to diffuse out of the pore structure. However, the restricted effects caused by these two factors are limited, most adsorbed gas molecules still can desorb and diffuse out of the pores when the gas pressure decreases. Therefore, the fact that $V_{L\text{-}ad}$ shows a positive relationship with $V_{L\text{-}de}$ is reasonable; meanwhile, **Figures 4A, E** show D_s shows a positive relationship with $V_{L\text{-}ad}$, so it is no wonder that $V_{L\text{-}de}$ increases with D_s increasing.

However, no correlation was found between D_s and $P_{L\text{-}ad}$ as well as between D_s and $P_{L\text{-}de}$ according to the fluctuation presented in **Figures 4B, D, F, H**.

Determination of Ad-/Desorption Hysteresis and Impact of D_s on Ad-/Desorption Hysteresis

Scholars in different fields, such as soil, rock, and high-molecular polymer, have ever proposed various hysteresis indexes for evaluating ad-/desorption hysteresis phenomenon based on the Freundlich index, the equilibrium concentration of solid phase, slope (Ran et al., 2003; Wu and Sun, 2010; Ding and Rice, 2011); however, they are not quite applicable to gas adsorption and desorption in coal (Wang G. et al., 2016). Wang et al. (2014) put forward an improved hysteresis index (IHI) based on the area formed by ad-/desorption isotherms, which has been proved to be effective in quantitatively characterizing the degree of gas ad-/desorption hysteresis in coal (Wang G. et al., 2016; Sun et al., 2020). Hence, IHI was adopted in this work, as shown by **Eqs 4–9**,

$$IHI = \frac{A_{hy}}{A_{hf}} = \frac{A_{de} - A_{ad}}{A_{sf} - A_{ad}} \times 100\%, \tag{4}$$

$$\begin{aligned} A_{ad} &= \int_0^{Pf} \frac{V_{L-ad}P}{P_{L-ad}+P}dP = V_{L-ad}\int_0^{Pf}\left(1 - \frac{P_{L-ad}}{P_{L-ad}+P}\right)dP \\ &= V_{L-ad}\left[P_f - P_{L-ad}\ln\left(1+\frac{P_f}{P_{L-ad}}\right)\right], \end{aligned} \tag{5}$$

$$\begin{aligned} A_{de} &= \int_0^{Pf}\left(\frac{V_{L-de}P}{P_{L-de}+P} + M\right)dP = V_{L-de}\int_0^{Pf}\left(1 - \frac{P_{L-de}}{P_{L-de}+P}\right)dP + MPf \\ &= V_{L-de}\left[P_f - P_{L-de}\ln\left(1+\frac{P_f}{P_{L-de}}\right)\right] + MP_f, \end{aligned} \tag{6}$$

$$A_{sf} = P_f\left(\frac{V_{L-de}P_f}{P_{L-ad}+P_f} + M\right), \tag{7}$$

$$A_{hy} = A_{de} - A_{ad}, \tag{8}$$

$$A_{hf} = A_{sf} - A_{ad}, \tag{9}$$

where A_{ad} and A_{de} stand for the zones below the adsorption and desorption isotherms; P_f stands for the final equilibrium pressure, MPa; A_{hy} represents the measured hysteresis area; and A_{hf} and A_{sf} represent the hysteresis area and the adsorption area in the fully irreversible case, respectively.

Figure 6 shows the IHI calculation of CO_2 and CH_4, and the results are listed in **Table 5**.

Jessen et al. (2008) have demonstrated that desorption isotherms depend on the initial pressure at the beginning of depressurization; therefore, when the final equilibrium pressure set in **Eqs 5–7** varies, ad-/desorption hysteresis varies as well. To avoid the possible error caused by the difference of the final equilibrium pressure of every sample, the final equilibrium pressures of CO_2 and CH_4 were uniformly set to 3.5 and 8 MPa for IHI calculation in this work. It should be noted that desorption points at 0 MPa were

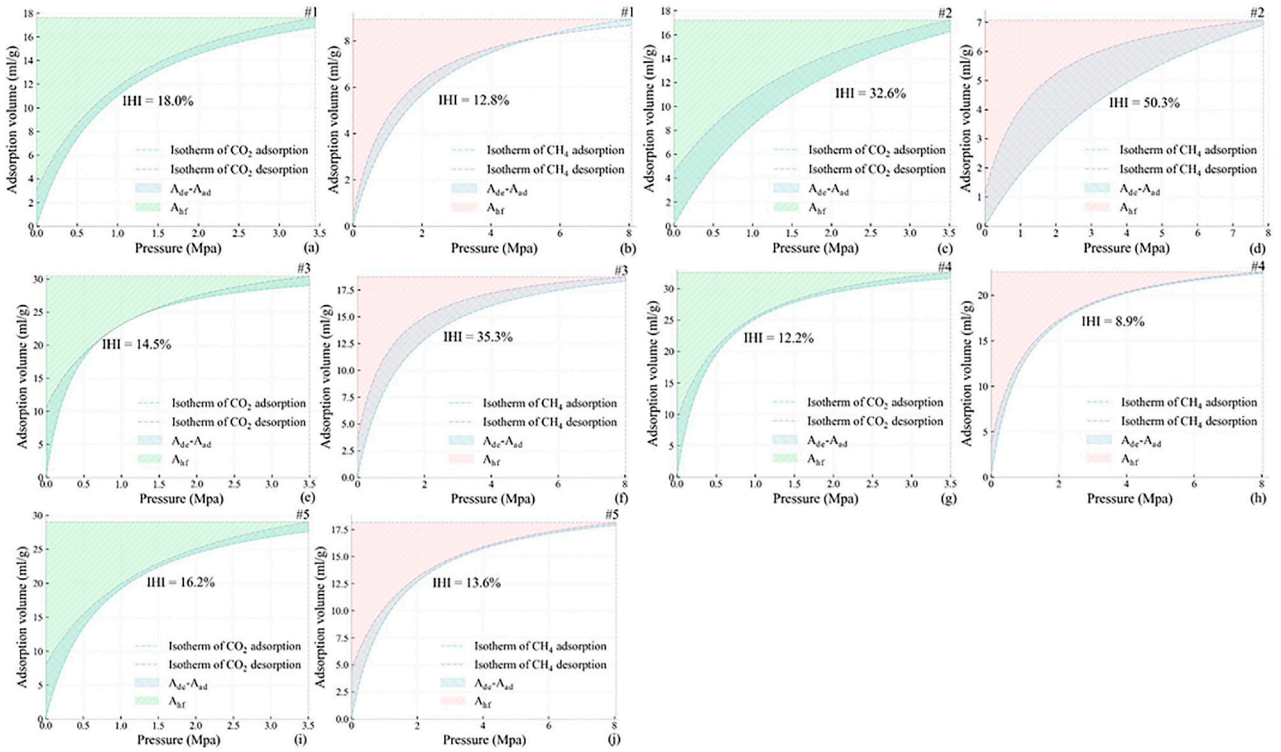

FIGURE 6 | IHI calculation. **(A)**, **(C)**, **(E)**, **(G),** and **(I)** represent CO_2 IHI calculation; **(B)**, **(D)**, **(F)**, **(H),** and **(J)** represent CH_4 IHI calculation.

TABLE 5 | IHI Results.

Sample	IHI (%)	
	CO_2	CH_4
#1	18.0	12.8
#2	32.6	50.3
#3	14.5	35.3
#4	12.2	8.9
#5	16.2	13.6

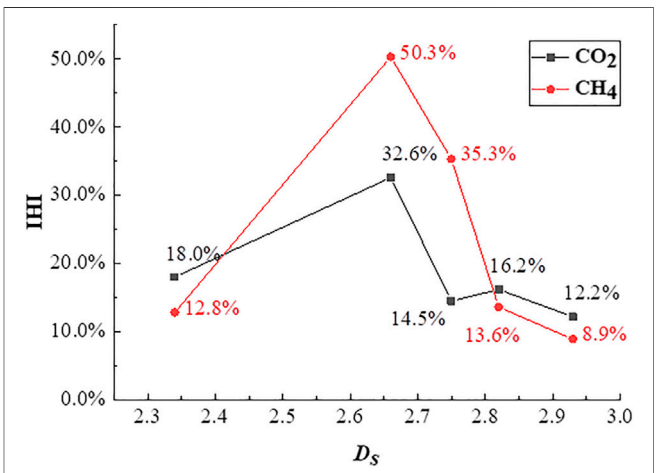

FIGURE 7 | D_s vs. IHI curves.

not measured in this work; to enable the adsorption and desorption isotherms to form a closed interval with the y axis and the vertical axis passed through (P_f, 0), the desorption isotherms were extended to the (0, M) point according to **Eq. 3**. Since the proposed IHI is calculated based on the area instead of a single point, a slight change at the end of desorption isotherms cannot significantly affect the calculation results of the IHI value; thus, the process of desorption isotherm extension is theoretically acceptable.

Figure 7 shows the relationship between D_s and IHI. It can be seen that for CO_2, IHI fluctuates with D_s changing. It first increases from 18.0 to 32.6% when D_s increases from 2.34 to 2.66, and then decreases to 14.5%, followed with a slight bounce to 16.1%, and finally drops to 12.2%. For CH_4, IHI rises to the maximum value of 50.3% when D_s increases from 2.34 to 2.66, and keeps falling when D_s varies between 2.66 and 2.93. In general, the curves of D_s vs. IHI for CO_2 and CH_4 are like an irreversible "V" shape.

As mentioned in *Determination of Langmuir Constants*, coal physical properties that can be directly reflected by D_s are the van der Waals force and the pore surface irregularity. Zhang et al. (2005) have reported that the adsorbed gas molecules on the pore surface of coal require a certain amount of energy to offset the van der Waals force so

that they can escape from the pore surface; therefore, the desorption process will lag behind adsorption to varying degrees. According to the viewpoint by Zhang et al. (2005), the stronger the van der Walls force is, the more obvious the ad-/desorption hysteresis is. Besides, Seri-Levy and Avnir (1993) have studied the effect of the heterogeneity of the pore surface on CH_4 ad-/desorption hysteresis. He demonstrated that the pore surface heterogeneity is sufficient to induce an ad-/desorption hysteresis loop and the degree of ad-/desorption hysteresis increases with the pore surface heterogeneity increasing. According to the statements by Zhang et al. (2005) and Seri-Levy and Avnir (1993), D_s and IHI are also more likely to present a positive relationship, but in this work, they present an irreversible "V-like" shape, primarily caused by that the ad-/desorption hysteresis in the sample with the D_s value 2.66 is rather dramatical, but the intrinsic mechanism of the irreversible "V-like" shape is hard to be explained by the existing theories and yields to be further investigated.

CONCLUSION

Fractal features of five coals were characterized by SAXS, the classic Langmuir model and the improved Langmuir model were adopted to characterize the gas adsorption and desorption capacities, and IHI was adopted to characterize the degree of gas ad-/desorption hysteresis. The evidence leads to the following conclusions:

1) Different samples show different surface fractal features with D_s values varying from 2.34 to 2.93.
2) The $V_{L\text{-}ad}$ and $V_{L\text{-}de}$ values of CO_2 are greater than those of CH_4, demonstrating that the adsorption and desorption capacities of CO_2 are stronger than those of CH_4. The $P_{L\text{-}ad}$ values of CH_4 are greater than those of CO_2, demonstrating that CH_4 is harder to be adsorbed on the coal pore surface than CO_2.
3) In the adsorption stage, D_s and $V_{L\text{-}ad}$ show a positive relationship for CH_4 and CO_2, which is attributed to the van der Waals force and available adsorption sites. In the desorption stage, D_s and $V_{L\text{-}de}$ show a positive relationship for CH_4 and CO_2 because most adsorbed gas molecules can desorb and diffuse out of the pores when the gas pressure decreases. No correlation was found between D_s and $P_{L\text{-}ad}$ as well as between D_s and $P_{L\text{-}de}$ on a basis of SAXS fractal theory.
4) The curves of D_s vs. IHI for CO_2 and CH_4 are like an irreversible "V" shape, primarily caused by the fact that the ad-/desorption hysteresis in the sample with the D_s value 2.66 is rather dramatical, but the intrinsic mechanism yields to be further studied.

DATA AVAILABILITY STATEMENT

The original contributions presented in the study are included in the article, further inquiries can be directed to the corresponding author.

AUTHOR CONTRIBUTIONS

YZ: Provide the experiment condition, design the experiment, theoretical analysis, revise the manuscript. CH: Conduct the experiment, draft the manuscript. YS: Theoretical analysis, revise the manuscript. YG: Data collection and figure drawing. HQ: Data collection and figure drawing. ZT: Conduct the experiment.

FUNDING

The research is financially sponsored by the National Natural Science Foundation of China (Grant Nos. U1910206, 51861145403, 51874312 and 52004293); the Open Project Program of Key Laboratory of Deep Earth Science and Engineering (Sichuan University), Ministry of Education (No. DESE 202004); the Fundamental Research Funds for the Central Universities (No. FRF-TP-20-034A1); the China Postdoctoral Science Foundation (No. 2018M641526); and the Yue Qi Distinguished Scholar Project of the China University of Mining and Technology (Beijing).

ACKNOWLEDGMENTS

The authors thank Zhihong Li, Guang Mo, and Wanxia Huang of the Beijing Synchrotron Radiation Laboratory (BSRF) for providing SAXS experimental facilities and for their suggestions in conducting experiments and data processing.

REFERENCES

Budinis, S., Krevor, S., Dowell, N. M., Brandon, N., and Hawkes, A. (2018). An Assessment of CCS Costs, Barriers and Potential. *Energ. Strategy Rev.* 22, 61–81. doi:10.1016/j.esr.2018.08.003

Chen, L., Jiang, Z., Wen, N., Gao, F., Wang, P., Ji, W., et al. (2017). Fractal Characteristics of Nanopores and Their Effect on Methane Adsorption Capacity in Shales. *Sci. Technol. Eng.* 53, 1689–1699. doi:10.1017/CBO9781107415324.004

Cui, X., Bustin, R. M., and Dipple, G. (2004). Selective Transport of CO2, CH4, and N2 in Coals: Insights from Modeling of Experimental Gas Adsorption Data. *Fuel* 83, 293–303. doi:10.1016/j.fuel.2003.09.001

Ding, G., and Rice, J. A. (2011). Effect of Lipids on Sorption/desorption Hysteresis in Natural Organic Matter. *Chemosphere* 84, 519–526. doi:10.1016/j.chemosphere.2011.03.009

Ekundayo, J. M., and Rezaee, R. (2019). Volumetric Measurements of Methane-Coal Adsorption and Desorption Isotherms-Effects of Equations of State and Implication for Initial Gas Reserves. *Energies* 12, 1–13. doi:10.3390/en12102022

Fan, J.-L., Xu, M., Li, F., Yang, L., and Zhang, X. (2018). Carbon Capture and Storage (CCS) Retrofit Potential of Coal-Fired Power Plants in China: The Technology Lock-In and Cost Optimization Perspective. *Appl. Energ.* 229, 326–334. doi:10.1016/j.apenergy.2018.07.117

Hammersley, A. P., Svensson, S. O., Hanfland, M., Fitch, A. N., and Hausermann, D. (1996). Two-dimensional Detector Software: From Real Detector to

Idealised Image or Two-Theta Scan. *High Press. Res.* 14, 235–248. doi:10.1080/08957959608201408

He, X., Cheng, Y., Hu, B., Wang, Z., Wang, C., Yi, M., et al. (2020). Effects of Coal Pore Structure on Methane-coal Sorption Hysteresis: An Experimental Investigation Based on Fractal Analysis and Hysteresis Evaluation. *Fuel* 269, 117438. doi:10.1016/j.fuel.2020.117438

He, X., Wang, E., and Lin, H. (1996). Coal Deformation and Fracture Mechanism under Pore Gas Action. *J. China Univ. Min Technol.* 25, 6–11. CNKI:SUN:ZGKD.0.1996-01-001.

Hou, X., Liu, S., Zhu, Y., and Yang, Y. (2020). Experimental and Theoretical Investigation on Sorption Kinetics and Hysteresis of Nitrogen, Methane, and Carbon Dioxide in Coals. *Fuel* 268, 117349. doi:10.1016/j.fuel.2020.117349

IEA (2017). *Energy Technology Perspective 2017*.

Jessen, K., Tang, G.-Q., and Kovscek, A. R. (2008). Laboratory and Simulation Investigation of Enhanced Coalbed Methane Recovery by Gas Injection. *Transp Porous Med.* 73, 141–159. doi:10.1007/s11242-007-9165-9

Langmuir, I. (1918). The Adsorption of Gases on Plane Surfaces of Glass, Mica and Platinum. *J. Am. Chem. Soc.* 40, 1361–1403. doi:10.1021/ja02242a004

Li, Z., Hao, Z., Pang, Y., and Gao, Y. (2015). Fractal Dimensions of Coal and Their Influence on Methane Adsorption. *J. China Coal Soc.* 40, 863–869. doi:10.13225/j.cnki.jccs.2014.3022

Liu, X., and Nie, B. (2016). Fractal Characteristics of Coal Samples Utilizing Image Analysis and Gas Adsorption. *Fuel* 182, 314–322. doi:10.1016/j.fuel.2016.05.110

Liu, Y., Li, X., and Bai, B. (2005). Preliminary Estimation of CO2 Storage Capacity of Coalbeds in China. *Chin. J. Rock Mech. Eng.* 16, 2947–2952. doi:10.3321/j.issn:1000-6915.2005.16.02310.1360/jos161833

Ma, D., Ma, W., and Lin, Y. B. (2012). Desorption Hysteresis Characteristics of CBM. *Meitan Xuebao/journal China Coal Soc.* 37, 1885–1889. doi:10.13225/j.cnki.jccs.2012.11.011

Ma, D., Zhang, S., and Lin, Y. (2011). Isothermal Adsorption and Desorption experiment of Coal and Experimental Results Accuracy Fitting. *J. China Coal Soc.* 36, 477–480. doi:10.13225/j.cnki.jccs.2011.03.006

Mares, T. E., Radliński, A. P., Moore, T. A., Cookson, D., Thiyagarajan, P., Ilavsky, J., et al. (2009). Assessing the Potential for CO2 Adsorption in a Subbituminous Coal, Huntly Coalfield, New Zealand, Using Small Angle Scattering Techniques. *Int. J. Coal Geology*. 77, 54–68. doi:10.1016/j.coal.2008.07.007

Nie, B., Wang, K., Fan, Y., Zhao, J., Zhang, L., Ju, Y., et al. (2021). Small Angle X-ray Scattering Test of Hami Coal Sample Nanostructure Parameters with Gas Adsorbed under Different Pressures. *J. Nanosci. Nanotechnol.* 21, 538–546. doi:10.1166/jnn.2021.18725

Niu, Q., Pan, J., Jin, Y., Wang, H., Li, M., Ji, Z., et al. (2019). Fractal Study of Adsorption-Pores in Pulverized Coals with Various Metamorphism Degrees Using N2 Adsorption, X-ray Scattering and Image Analysis Methods. *J. Pet. Sci. Eng.* 176, 584–593. doi:10.1016/j.petrol.2019.01.107

Pan, J., Niu, Q., Wang, K., Shi, X., and Li, M. (2016). The Closed Pores of Tectonically Deformed Coal Studied by Small-Angle X-ray Scattering and Liquid Nitrogen Adsorption. *Microporous Mesoporous Mater.* 224, 245–252. doi:10.1016/j.micromeso.2015.11.057

Qi, H., Ma, J., and Wong, P.-z. (2002). Adsorption Isotherms of Fractal Surfaces. *Colloids Surf. A: Physicochemical Eng. Aspects* 206, 401–407. doi:10.1016/S0927-7757(02)00063-8

Ran, Y., Xiao, B., Fu, J., and Sheng, G. (2003). Sorption and Desorption Hysteresis of Organic Contaminants by Kerogen in a sandy Aquifer Material. *Chemosphere* 50, 1365–1376. doi:10.1016/S0045-6535(02)00762-2

Reich, M. H., Snook, I. K., and Wagenfeld, H. K. (1992). A Fractal Interpretation of the Effect of Drying on the Pore Structure of Victorian Brown Coal. *Fuel* 71, 669–672. doi:10.1016/0016-2361(92)90170-S

Sander, R., Pan, Z., Connell, L. D., Camilleri, M., and Heryanto, D. (20162016). Experimental Investigation of Gas Diffusion in Coal - Comparison between Crushed and Intact Core Samples. *PE Asia Pac. Oil Gas Conf. Exhibition*. doi:10.2118/182466-MS

Seri-Levy, A., and Avnir, D. (1993). Effects of Heterogeneous Surface Geometry on Adsorption. *Langmuir* 9, 3067–3076. doi:10.1021/la00035a054

Song, X., Tang, Y., Li, W., Zeng, F., and Xiang, J. (2014). Pore Structure in Tectonically Deformed Coals by Small Angle X-ray Scattering. *J. China Coal Soc.* 39, 719–724. doi:10.13225/j.cnki.jccs.2013.1932

Sun, W., Feng, Y., Jiang, C., and Chu, W. (2015). Fractal Characterization and Methane Adsorption Features of Coal Particles Taken from Shallow and Deep Coalmine Layers. *Fuel* 155, 7–13. doi:10.1016/j.fuel.2015.03.083

Sun, Y., Zhao, Y., and Yuan, L. (2018). CO2-ECBM in Coal Nanostructure: Modelling and Simulation. *J. Nat. Gas Sci. Eng.* 54, 202–215. doi:10.1016/j.jngse.2018.04.007

Sun, Y., Zhao, Y., and Yuan, L. (2020). Impact of Coal Composition and Pore Structure on Gas Adsorption: a Study Based on a Synchrotron Radiation Facility. *Greenhouse Gas Sci. Technol.* 10, 116–129. doi:10.1002/ghg.1935

Syed, R., Sen, D., Mani Krishna, K. V., and Ghosh, S. K. (2018). Fabrication of Highly Ordered Nanoporous Alumina Membranes: Probing Microstructures by SAXS, FESEM and AFM. *Microporous Mesoporous Mater.* 264, 13–21. doi:10.1016/j.micromeso.2017.12.034

Tan, Y., Pan, Z., Liu, J., Kang, J., Zhou, F., Connell, L. D., et al. (2018). Experimental Study of Impact of Anisotropy and Heterogeneity on Gas Flow in Coal. Part I: Diffusion and Adsorption. *Fuel* 232, 444–453. doi:10.1016/j.fuel.2018.05.173

Wang, G. (2015). *Adsorption and Desorption Hysteresis of Coal Seam Gas and its Influence on Gas Permeability*. Beijing: China University of Mining and Technology. [dissertation]. [China (LP)].

Wang, G., Ren, T., Qi, Q., Wang, K., and Zhang, L. (2016a). Mechanism of Adsorption-Desorption Hysteresis and its Influence on Deep CBM Recovery. *J. China Coal Soc.* 41, 49–56. doi:10.13225/j.cnki.jccs.2015.9022

Wang, K., Wang, G., Ren, T., and Cheng, Y. (2014). Methane and CO 2 Sorption Hysteresis on Coal: A Critical Review. *Int. J. Coal Geology*. 132, 60–80. doi:10.1016/j.coal.2014.08.004

Wang, Y., Li, Z., Kong, J., Chang, L., Li, D., and Lv, B. (2021). *In-situ* SAXS Study on Fractal of Jincheng Anthracite during High-Temperature Carbonisation. *Phil. Mag. Lett.* 101, 320–329. doi:10.1080/09500839.2021.1936259

Wang, Y., Zhu, Y., Liu, S., and Zhang, R. (2016b). Pore Characterization and its Impact on Methane Adsorption Capacity for Organic-Rich marine Shales. *Fuel* 181, 227–237. doi:10.1016/j.fuel.2016.04.082

Wijnen, P. W. J. G., Beelen, T. P. M., Rummens, K. P. J., Saeijs, H. C. P. L., and van Santen, R. A. (1991). Silica Gel from Water Glass: a SAXS Study of the Formation and Ageing of Fractal Aggregates. *J. Appl. Cryst.* 24, 759–764. doi:10.1107/S0021889891000924

Wu, W., and Sun, H. (2010). Sorption-desorption Hysteresis of Phenanthrene - Effect of Nanopores, Solute Concentration, and Salinity. *Chemosphere* 81, 961–967. doi:10.1016/j.chemosphere.2010.07.051

Xie, F., Li, D., Li, Z., Li, Z., Mo, G., and Lv, B. (2019). Small-angle X-ray Scattering Study on the Fractal Structure of Solid Products of Bituminous Coal at Different Carbonization Temperatures. *Phil. Mag. Lett.* 99, 95–101. doi:10.1080/09500839.2019.1628366

Xu, F., Wang, B., Zhao, X., Yun, J., Zhang, S., Wang, H., et al. (2021). Thoughts and Suggestions on Promoting High Quality Development of China's CBM Business under the Goal of "Double Carbon. *China Pet. Explor.* 26 (3), 9–18. doi:10.3969/j.issn.1672-7703.2021.03.002

Yang, Y., and Liu, S. (2019). Estimation and Modeling of Pressure-dependent Gas Diffusion Coefficient for Coal: A Fractal Theory-Based Approach. *Fuel* 253, 588–606. doi:10.1016/j.fuel.2019.05.009

Yao, Y., Liu, D., Tang, D., Tang, S., and Huang, W. (2008). Fractal Characterization of Adsorption-Pores of Coals from North China: An Investigation on CH4 Adsorption Capacity of Coals. *Int. J. Coal Geology*. 73, 27–42. doi:10.1016/j.coal.2007.07.003

Yin, T., Liu, D., Cai, Y., and Zhou, Y. (2019). Methane Adsorption Constrained by Pore Structure in High-Rank Coals Using FESEM, CO2 Adsorption, and NMRC Techniques. *Energy Sci. Eng.* 7, 255–271. doi:10.1002/ese3.275

Zhang, L., Ye, Z., Li, M., Zhang, C., Bai, Q., and Wang, C. (2018). The Binary Gas Sorption in the Bituminous Coal of the Huaibei Coalfield in China. *Adsorption Sci. Tech.* 36, 1612–1628. doi:10.1177/0263617418798125

Zhang, R., and Liu, S. (2017). Experimental and Theoretical Characterization of Methane and CO2 Sorption Hysteresis in Coals Based on Langmuir Desorption. *Int. J. Coal Geology*. 171, 49–60. doi:10.1016/j.coal.2016.12.007

Zhang, S., Ye, J., Tang, S., Ma, D., and Huo, Y. (2005). Theoretical Analysis of Coal-Methane Adsorption/desorption Mechanism and its Reversibility experiment. *Nat. Gas Industry* 25, 1–29. doi:10.1016/j.molcatb.2005.02.001

Zhang, X. G., Ranjith, P. G., Perera, M. S. A., Ranathunga, A. S., and Haque, A. (2016). Gas Transportation and Enhanced Coalbed Methane Recovery

Processes in Deep Coal Seams: A Review. *Energy Fuels* 30, 8832–8849. doi:10.1021/acs.energyfuels.6b01720

Zhao, Y., Liu, S., Elsworth, D., Jiang, Y., and Zhu, J. (2014). Pore Structure Characterization of Coal by Synchrotron Small-Angle X-ray Scattering and Transmission Electron Microscopy. *Energy Fuels* 28, 3704–3711. doi:10.1021/ef500487d

Zhao, Y., and Peng, L. (2017). Investigation on the Size and Fractal Dimension of Nano-Pore in Coals by Synchrotron Small Angle X-ray Scattering. *Chin. Sci. Bull.* 62, 2416–2427. doi:10.1360/N972016-00970

Zhao, Y., Peng, L., Liu, S., Cao, B., Sun, Y., and Hou, B. (2019). Pore Structure Characterization of Shales Using Synchrotron SAXS and NMR Cryoporometry. *Mar. Pet. Geology*. 102, 116–125. doi:10.1016/j.marpetgeo.2018.12.041

Zhou, Y., Zhang, R., Wang, J., Huang, J., Li, X., and Wu, J. (2020). Desorption Hysteresis of CO2 and CH4 in Different Coals with Cyclic Desorption Experiments. *J. CO2 Utilization* 40, 101200. doi:10.1016/j.jcou.2020.101200

Conflict of Interest: The authors declare that the research was conducted in the absence of any commercial or financial relationships that could be construed as a potential conflict of interest.